



# Double Acting Compression Mechanism (DACM) for Piezoelectric Vibration Energy Harvesting in 33-Mode Operation

Byung C. Jung<sup>1</sup> · Heonjun Yoon<sup>2</sup>

Received: 12 June 2018 / Revised: 18 October 2018 / Accepted: 29 January 2019 / Published online: 12 February 2019  
© Korean Society for Precision Engineering 2019

## Abstract

Piezoelectric vibration energy harvesting (PVEH) has been emerged as an alternative solution for sustainable powering to electronics. It has been well known that a PZT stack operating in 33-mode has higher mechanical to electrical energy conversion efficiency and higher mechanical reliability, compared to a cantilevered PZT bimorph operating in 31-mode. However, there are two challenges to improve the output performance of a PZT stack at a low frequency environment. First, the lower tensile strength of a PZT stack compared to the compressive strength makes it difficult to fully utilize maximum strain at harsh vibration conditions. Second, the relatively high stiffness of a PZT stack prevents being resonant with a base structure vibrating at a low frequency. To solve these challenges, this study thus proposes a double acting compression mechanism (DACM)-based PVEH stack operating in 33-mode. The DACM-based PVEH stack can convert mechanical vibration into elevated two-way compressive loading. The analytic model is used to investigate the electroelastic behaviors of the DACM-based PVEH device at given vibration conditions. The comparative study is performed to verify the effectiveness of the DACM-based PVEH stack over other mechanisms. It can be concluded that the DACM-based PVEH stack enables to generate higher power with the same volume of PZT using elevated two-way compressive loading.

**Keywords** Piezoelectric vibration energy harvesting · PZT stack · 33-Mode · Double acting compression mechanism

## List of Symbols

$M$	Mass of a weight
$c$	Damping coefficient
$k$	Stiffness of a spring
$x$	Displacement of a damped single degree-of-freedom system
$y$	Displacement of base excitation
$X$	Maximum displacement
$Y$	Maximum displacement of base excitation
$\omega$	Angular natural frequency
$\zeta$	Damping ratio
$F_T$	Maximum compressive load applied to a PZT stack

$r$	Frequency ratio
$S$	Strain
$T$	Stress
$E$	Elastic field
$D$	Electric displacement
$s^E$	Elastic compliance at constant electric field
$d$	Piezoelectric coupling coefficient
$\epsilon$	Dielectric permittivity
$x_{cs}$	Displacement of a PZT stack
$h$	Thickness of a piezoelectric layer
$A_{cs}$	Cross-sectional area
$F$	Actuation force to a PZT stack
$Q$	Electric charge
$V$	Output voltage
$n$	The number of piezoelectric layers
$L$	Length of a PZT stack
$P$	Output electric power
$R$	External electrical resistance
$C$	Capacitance

Byung Chang Jung and Heonjun Yoon contributed equally to this work as the first author.

✉ Byung C. Jung  
bcjung@kimm.re.kr

<sup>1</sup> Department of System Dynamics, Korea Institute of Machinery and Materials, 156 Gajeongbuk-ro, Yuseong-gu, Daejeon 34103, Republic of Korea

<sup>2</sup> Department of Mechanical and Aerospace Engineering, Seoul National University, 1 Gwanak-ro, Gwanak-gu, Seoul 08826, Republic of Korea

## 1 Introduction

Piezoelectric vibration energy harvesting (PVEH) refers to a technology that can capture ambient, otherwise wasted, vibration energy and convert it into usable electricity [1–11]. A typical type of a PVEH device is a cantilevered unimorph/bimorph beam, which operates in 31-mode (the direction of applied stress is perpendicular to the poling direction) [12–17]. Another type is a stack, which operates in 33-mode (the direction of applied stress is the same with the poling direction). However, it is well known that a piezoelectric stack is more durable in high force environments and has higher mechanical to electrical energy conversion efficiency [18–24]. Xu et al. [19] revealed that a piezoelectric stack has 35% energy conversion efficiency (mechanical to electrical), which is over four times higher than other devices (less than 7.5%); and concluded that the output electric power is significantly higher than that generated by a cantilevered PVEH device with a similar weight and size at both resonance and off-resonance modes due to high energy conversion efficiency and larger equivalent piezoelectric coefficient. Feenstra et al. [20] developed a device to mechanically amplify force input into a PZT stack for generating electric energy from a backpack. Song et al. [21] showed that a thin multilayer ceramic in a stack configuration was beneficial to charge the battery and to power a wireless sensor node since it can generate the larger current by scarifying the voltage and decrease the impedance of PVEH device by increasing the number of piezoelectric layers. Lee et al. [23] and Zhao [24] investigated the energy harvesting performance of a PZT stack under a shock event and a random vibration condition, respectively.

However, there are two challenges to improve the energy harvesting performance of a PZT stack at a low frequency environment. The first challenge is that the tensile strength of a PZT stack is much lower than its compressive strength, as shown in Table 1. The low tensile strength of a PZT stack makes it difficult to fully utilize maximum strain at harsh loading conditions. The second challenge is that the high stiffness of a PZT stack prevents being resonant with base structures vibrating at a low frequency. As an innovative

**Table 1** Tensile and compressive strength of PZT materials

Material	Tensile strength (MPa)		Compressive strength (MPa)
	Static	Dynamic	
PZT-5A [25]	75.8	27.6	> 517
	100	–	> 600
PZT stack [26]	4.9	–	880
PZT-5H [27]	–	14	–

design, therefore, this paper proposes a double acting compression mechanism (DACM) for PVEH in a stack (33-mode) configuration. The DACM converts mechanical vibration into elevated two-way compressive loads.

In Sect. 2, a working principle of the DACM-based PVEH stack and its analytical model to predict the output electric power are presented. Section 3 provides a comparative study between the DACM-based PVEH stack and a cantilevered bimorph. In Sect. 4, a comparative study between the DACM-based PVEH and conventional PZT stacks is described. Finally, the conclusion of this study is outlined in Sect. 5.

## 2 Double Acting Compression Mechanism (DACM)-Based Piezoelectric Vibration Energy Harvesting

### 2.1 Working Principle of the DACM

Figure 1 shows a schematic of the DACM-based PVEH stack, which consists of a cylindrical housing, a PZT stack, a mass, a spring, a protector, guide caps, and guide blocks. The cylindrical housing, which is attached to the top surface of the vibrating structure, protects the PZT stack from environmental hazards. The non-conductive protector joins the PZT stack to the spring. The two guide caps are attached to the top of the PZT stack and the bottom of the spring, respectively. The guide blocks can be fastened on the mass or the inner surface of the cylindrical housing. The guide caps and blocks constrain a movement in a lateral direction, and allow the DACM-based PVEH stack to move in a vertical direction. The guide caps and blocks are assumed to be made of low friction materials, such as Teflon, to minimize the dissipation by coulomb friction.

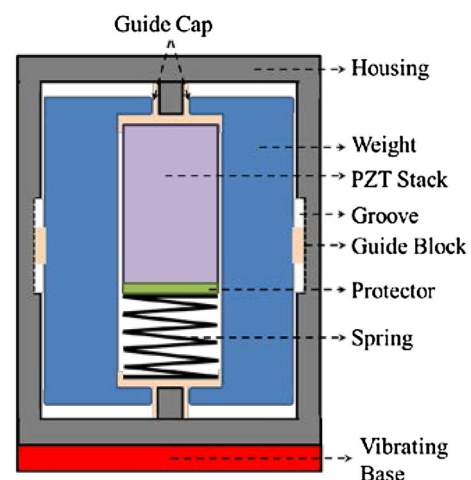


**Fig. 1** Cross-section of the DACM-based PVEH stack

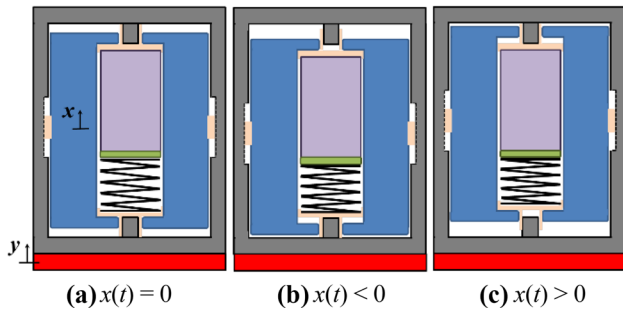


Fig. 2 Working mechanism of the DACM-based PVEH stack

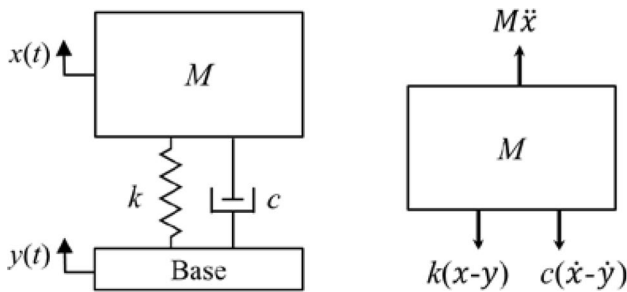


Fig. 3 Free body diagram for a motion of the weight

Figure 2 illustrates a harmonic motion of the mass, denoted by  $x(t)$ , relative to sinusoidal base excitation of the vibrating base, denoted by  $Y(t) = Y \sin(\omega_b t)$ , where  $Y$  denotes the maximum displacement of base excitation and  $\omega_b$  denotes a driving angular frequency. Two-way compressive loads, which are equal to the reaction forces of a compressive spring, are applied to a PZT stack according to the harmonic motion of the weight.

The applied dynamic force can be calculated by solving the equation of motion for the weight. Figure 3 shows the free body diagram about the motion of the weight, denoted by  $x(t)$ . The equation of motion for the damped SDOF system can be expressed as:

$$M\ddot{x}(t) + c\dot{x}(t) + kx(t) = cY\omega_b \cos(\omega_b t) + kY \sin(\omega_b t), \quad (1)$$

where  $M$  denotes the mass of the weight;  $c$  denotes the damping coefficient; and  $k$  is the stiffness.

By solving Eq. (1), the displacement of the weight, denoted by  $x(t)$ , can be obtained as [28]:

$$x(t) = \omega Y \left[ \frac{\omega^2 + (2\zeta\omega_b)^2}{(\omega^2 - \omega_b^2)^2 + (2\zeta\omega\omega_b)^2} \right]^{0.5} \cos(\omega_b t - \phi_1 - \phi_2),$$

$$\phi_1 = \tan^{-1} \left( \frac{2\zeta\omega\omega_b}{\omega^2 - \omega_b^2} \right),$$

$$\phi_2 = \tan^{-1} \left( \frac{\omega}{2\zeta\omega_b} \right), \quad (2)$$

where  $\omega$  and  $\zeta$  are angular natural frequency and damping ratio. The displacement transmissibility and the ratio of the maximum force to the input displacement (force) can be obtained, respectively, as:

$$\frac{X}{Y} = \left[ \frac{\omega^2 + (2\zeta\omega_b)^2}{(\omega^2 - \omega_b^2)^2 + (2\zeta\omega\omega_b)^2} \right]^{0.5}, \quad (3)$$

$$\frac{F_T}{kY} = \left( \frac{\omega_b}{\omega} \right)^2 \left[ \frac{\omega^2 + (2\zeta\omega_b)^2}{(\omega^2 - \omega_b^2)^2 + (2\zeta\omega\omega_b)^2} \right]^{0.5},$$

where  $X$  and  $Y$  are the maximum displacement of  $x(t)$  and  $y(t)$ ; and  $F_T$  is the maximum compressive load applied to a PZT stack.

### 2.2 Electroelastically-Coupled Analytic Model of the DACM-Based PVEH stack

Feenstra et al. developed an electroelastically-coupled analytical model of the PZT stack [20]. In this study, this electroelastically-coupled analytical model is used to elucidate the electroelastic behaviors of the DACM-based PVEH stack. The linear constitutive relations for PZT are given as:

$$S_3 = s_{33}^E T_3 + d_{33} E_3, \quad (4)$$

$$D_3 = d_{33} T_3 + \epsilon_{33}^T E_3, \quad (5)$$

where  $S_3$  is strain;  $T_3$  is stress;  $E_3$  is the electric field;  $D_3$  is the electric displacement;  $s_{33}^E$  is the elastic compliance at the constant electric field;  $d_{33}$  is the piezoelectric coupling coefficient; and  $\epsilon_{33}^T$  is the dielectric permittivity at constant stress. Both the poling and force directions are the three-axis. By assuming that the force is uniformly applied on the surface of the piezoelectric layer, the constitutive relations can be simplified as:

$$S_3 = \frac{x(t)}{L}, D_3 = \frac{Q}{A_{cs}}, T_3 = \frac{F(t)}{A_{cs}}, E_3 = \frac{v(t)}{h}, \quad (6)$$

where  $x(t)$  is the displacement;  $h$  is the thickness of a piezoelectric layer;  $A_{cs}$  is the cross-sectional area;  $L$  is the length of a PZT stack ( $L = nh$ );  $F(t)$  is the force applied to a PZT

stack;  $Q_3$  is the electric charge; and  $v(t)$  is the output voltage. By considering the number of piezoelectric layers,  $n$ , and assuming that the applied compressive force to all piezoelectric layers is identical, the capacitance, compliance and Eq. (6) can be expressed as:

$$C_{st} = n\epsilon_{33}^T \frac{A_{cs}}{h}, S_{3,st} = \frac{x_{cs}}{nh}, D_{3,st} = \frac{Q_{3,cs}}{nA_{cs}}, \quad (7)$$

$$T_{3,st} = T_3, E_{3,st} = E_3, s_{33}^E = s_{33,st}^E,$$

where the subscript ‘st’ represents a PZT stack. By substituting Eq. (7) into Eqs. (4) and (5), the linear constitutive relations for PZT can be rewritten in terms of the displacement and the electric charge as:

$$x_{st}(t) = \frac{Ls_{33}^E}{A_{cs}}F(t) + \frac{d_{33}L}{h}v(t), \quad (8)$$

$$Q_{3,st}(t) = nd_{33}F(t) + C_{st}v(t). \quad (9)$$

It is assumed that the cross-sectional area of each piezoelectric layer is the same with that of a PZT stack. The displacement of a PZT stack by a dynamic load ( $F_d$ ) can be expressed with the SDOF model as:

$$m_{st}\ddot{x}_{st}(t) + c_{st}\dot{x}_{st}(t) + F(t) = F_d(t), \quad (10)$$

where  $m_{st}$  and  $c_{st}$  are the mass and damping coefficient of a PZT stack.

By applying Eqs. (8), (10) can be expressed as:

$$m_{st}\ddot{x}_{st}(t) + c_{st}\dot{x}_{st}(t) + \frac{A_{cs}}{Ls_{33,st}^E}x_{st}(t) - \frac{d_{33}A_{cs}}{hs_{33,st}^E C_{st}}Q_{3,st}(t) = F_d(t), \quad (11)$$

when an external electrical resistance, denoted by  $R$ , is connected to the PZT stack, an electric boundary condition can be defined as:

$$v(t) = -R\dot{Q}(t). \quad (12)$$

Then, Eq. (9) can be written by differentiating with respect to time results as:

$$\dot{v}(t) + \frac{1}{RC_{st}}v(t) + \frac{d_{33}A_{cs}}{hs_{33,st}^E C_{st}}\dot{x}_{st}(t) = 0. \quad (13)$$

In order to calculate the displacement of a PZT stack and the corresponding output voltage, Eqs. (11) and (13) can be

**Table 2** Material properties of the DACM-based PVEH stack

Property	Value	Unit
$d_{33}$	650	pm/V
$k_{33}$	0.75	–
$s_{33}^E$	20	pm <sup>2</sup> /N
$\epsilon_{33}^T/\epsilon_0$	3800	–
$\epsilon_0$	8.8542	pF/m
$C_{st}$	1600	nF
Compressive strength	880	MPa
Tensile strength	4.9	MPa
Young’s modulus	44	GPa
Poisson ratio	0.34	–
Stiffness	58	MN/m

**Table 3** Material properties of the cantilevered bimorph

Property	Value
PZT-5H [26]	
$d_{31}$	320 pC/N
$d_{33}$	650 pC/N
Density	7800 kg/m <sup>3</sup>
$\epsilon_{33}^T$	33.65 nF/m
$s_{11}^E$	16.13 pm <sup>2</sup> /N
$s_{33}^E$	20
Center shim (Brass) [13]	
Elastic modulus	126.5 GPa
Density	9133 kg/m <sup>3</sup>

rewritten in a state space form in terms of the state variables as:

$$\begin{Bmatrix} \dot{x} \\ \dot{\ddot{x}} \\ \dot{v} \end{Bmatrix} = \begin{bmatrix} 0 & 1 & 0 \\ -\frac{A_{cs}}{m_{st}Ls_{33,st}^E} & -\frac{C_{st}}{m_{st}} & \frac{d_{33}A_{cs}}{hs_{33,st}^E m_{st}} \\ 0 & -\frac{d_{33}A_{cs}}{hs_{33,st}^E C_{st}} & \frac{1}{RC_{st}} \end{bmatrix} \begin{Bmatrix} x \\ \ddot{x} \\ v \end{Bmatrix} + \begin{Bmatrix} 0 \\ \frac{1}{m_{st}} \\ 0 \end{Bmatrix} [F_d(t)]. \quad (14)$$

Finally, the output electric power can be obtained as:

$$P(t) = \frac{v^2(t)}{R}. \quad (15)$$

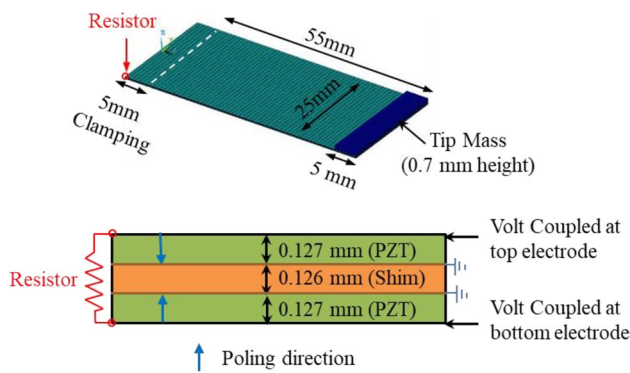


Fig. 4 Finite element model of the cantilevered bimorph

### 3 Comparative Study 1: DACM-Based PVEH Stack and Cantilevered Bimorph

In this section, the output performances of the DACM-based PVEH stack are compared with those of a cantilevered bimorph. It is assumed that the overall volumes of piezoelectric layers are equal to each other for all cases. In this study, PZT-5H (TS18-H5-104, Piezo Ceramic [26]) was used as a material of the piezoelectric layer. The material properties of the DACM-based PVEH stack and cantilevered bimorph are listed in Tables 2 and 3, respectively. It is worth pointing out that the compressive strength (880 MPa) of the PZT stack is about 180 times greater than the tensile strength (4.9 MPa).

The electroelastically-coupled analytical model presented in Sect. 2 is used to calculate the output performances of the DACM-based PVEH stack, while a finite element (FE) model described in Fig. 4 is used to analyze the cantilevered bimorph. The FE model is developed by using ANSYS software. The piezoelectric layers and center shim are modeled by using SOLID5 and SOLID45 elements, respectively. The poling direction of the piezoelectric layers is modeled as shown in Fig. 4. The electrodes covering the centre shim are grounded. The voltage degree of freedom for the top and bottom electrodes are connected

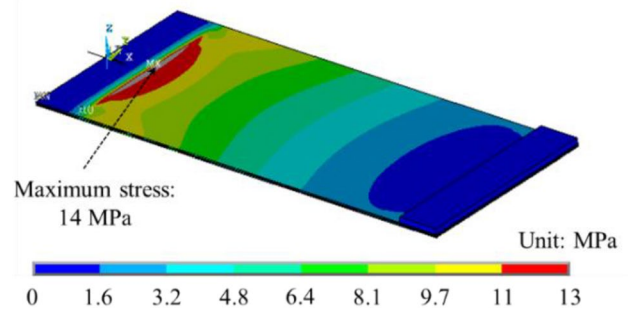


Fig. 5 Stress distribution of the cantilevered bimorph

to a resistor. As a tip mass, a copper block (length: 5 mm, width: 25 mm, thickness: 0.7 mm) is modeled to make the cantilevered bimorph be resonant with the excitation frequency of 60 Hz.

The simulation cases considered in this study are summarized in Table 4. For the cantilevered bimorph (case I), two piezoelectric layers are used in a series connection. The tensile stress constraint of 14 MPa is imposed to avoid mechanical failure. On the other hand, for the DACM-based PVEH device (cases II and III), the number of the piezoelectric layers is 110. It should be noted that the compressive stress constraint of 88 MPa is imposed in the case III, while it does not in the case II. It is worth pointing out that the natural frequency of the DACM-based PVEH stack can be controlled by changing the magnitudes of the mass and stiffness to be resonant with the excitation frequency of 60 Hz.

To satisfy the stress constraint for the case I, the acceleration amplitude of base excitation is set to be 0.43 g, which induces the maximum stress (14 MPa) of the cantilevered bimorph near the clamping part, as shown in Fig. 5. For the comparison, the acceleration amplitude of 0.43 g is applied for the cases II and III, as well. For all cases, the damping ratio is assumed to be 0.0198.

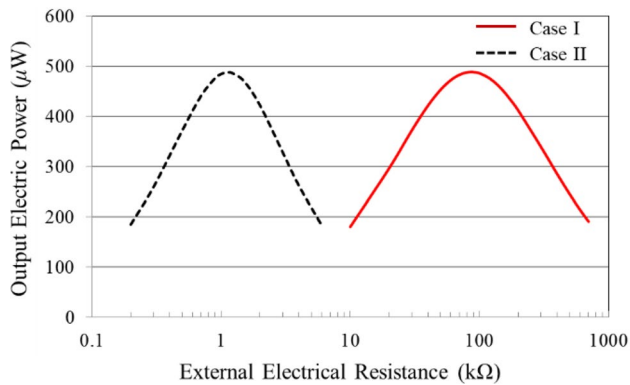
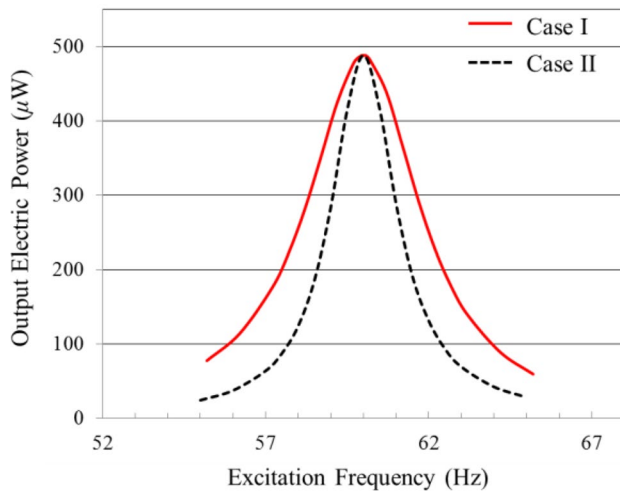
The simulation results for the cases I, II, and III are summarized in Table 5. As the purely resistive impedance matching condition to generate the maximum output electric power of 0.488 mW, the optimal external electrical resistances of the cantilevered bimorph (case I) and DACM-based

Table 4 Simulation cases: cantilevered bimorph versus DACM-based PVEH stack

	Case I	Case II	Case III
Mechanism	Cantilevered bimorph	DACM-based PVEH stack	
Geometric dimensions	Length: 55 mm Width: 25 mm Thickness: 0.127 mm 2 PZT layers	Length: 5 mm Width: 5 mm Thickness: 0.127 mm 110 PZT layers stacked	
Stress constraint	14 MPa (Tensile)	–	88 MPa (Compressive)
Damping ratio	0.0198 [13]		
Frequency	60 Hz [29]		
Acceleration amplitude	0.43 g		

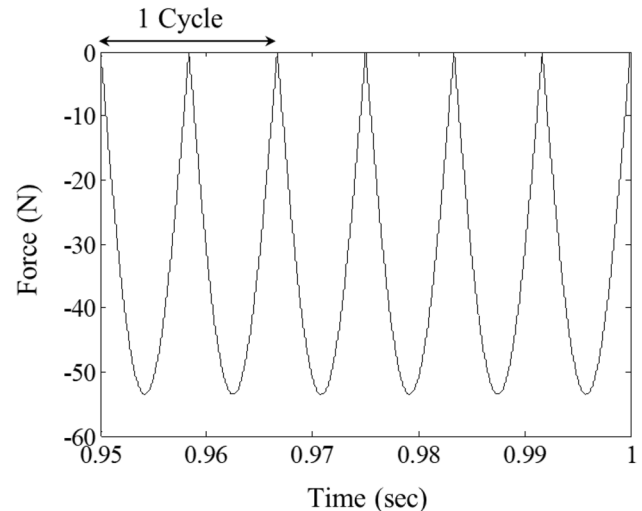
**Table 5** Simulation results: cantilevered bimorph versus DACM-based PVEH stack

	Case I	Case II	Case III
Maximum stress	14 MPa	2.02 MPa	88 MPa
Maximum compressive load	–	53.5 N	2323 N
Output voltage range	$\pm 9.3$ V	$-1.30$ V $\sim$ $+0.93$ V	$-58$ V $\sim$ $+40$ V
Output electric power (time average)	0.488 mW	0.488 mW	919 mW

**Fig. 6** Output electric power with respect to external electrical resistances: Cases I and II**Fig. 7** Frequency response for the output electric power: Cases I and II

PVEH stack (case II) are 88 k $\Omega$  and 1.13 k $\Omega$ , respectively. Figure 6 shows the output electric power with respect to the external electrical resistance for the cases I and II. Here, it is worth pointing out that the output electric power is calculated in an average sense for one cycle of the dynamic force, rather than a peak value.

When the acceleration amplitude of 0.43 g is applied to the DACM-based PVEH stack, the maximum stress of the case II is 2.02 MPa, which is much smaller than that of the

**Fig. 8** Dynamic force applied to the DACM-based PVEH stack (case II)

case I. This implies that the DACM-based PVEH stack (case II) is more reliable than the cantilevered bimorph against mechanical failure, while achieving the same maximum output electric power of 0.488 mW. Figure 7 shows the frequency responses for the cases I and II. The cantilevered bimorph (case I) has a relatively broader bandwidth than the DACM-based PVEH stack (case II), which means that the former would be robust to random excitation. It should be noted that the values of the output electric power at each excitation frequency in Figs. 6 and 7 are calculated by taking a time average for one cycle.

Figure 8 shows the dynamic force applied to the DACM-based PVEH stack (case II). The maximum compressive load is 53.5 N. It is worth noticing that two peak values of 53.5 N appear per one cycle, since the DACM converts base excitation into elevated two-way compressive loads. Figure 9 shows the simulation results of the case II. The output voltage generated by the DACM-based PVEH stack ranges from  $-1.30$  V to  $0.93$  V. Although the volume of the piezoelectric layers for the case II is the same with those for the case I, the total size of the DACM-based PVEH stack might be larger than that of the cantilevered bimorph due to the mass. However, the cantilevered bimorph requires

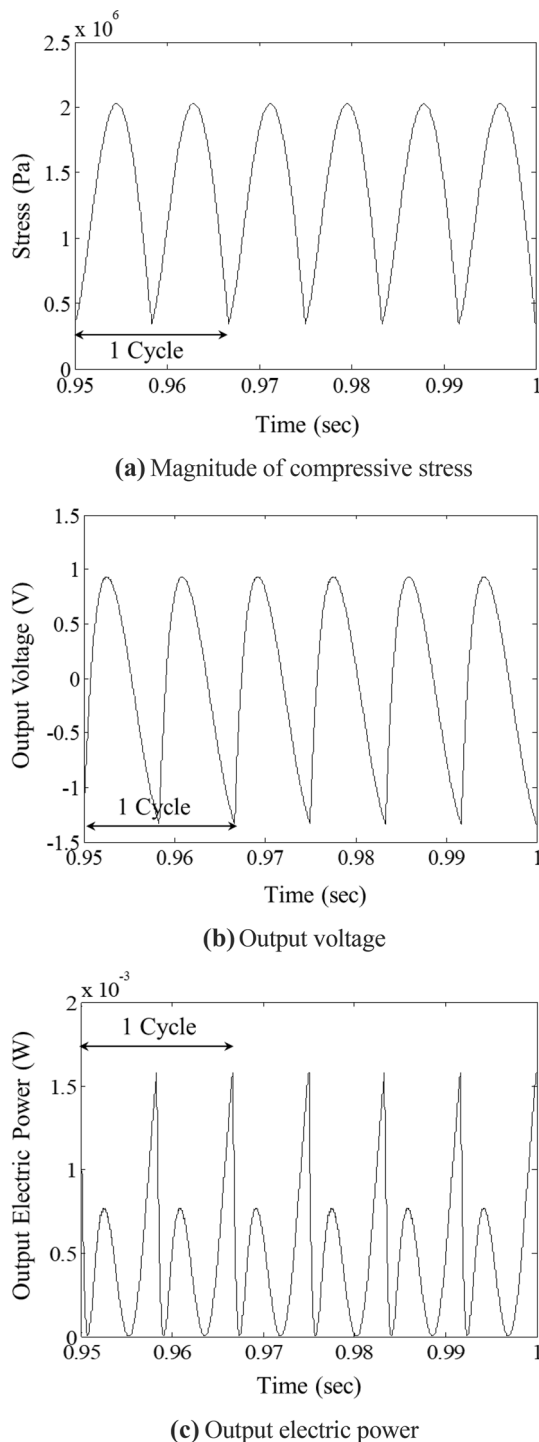


**Fig. 9** Simulation results of the DACM-based PVEH stack (case II)

additional spaces for the clamping part and operating volume of the tip displacement.

For the case III, the maximum compressive load is 1930 N, which induces the maximum stress of 88 MPa equal to the compressive strength of the PZT stack by considering a safety factor of ten. Under this compressive load,

the output electric power generated by the DACM-based PVEH stack is 919 mW at the optimal external electrical resistance of 1.13 k $\Omega$ . In summary, the DACM-based PVEH stack can exploit effectively the large magnitude of forces under the stress constraint on the compressive strength of the PZT stack, compared to the cantilevered bimorph that is constrained by the tensile strength. This implies that the DACM-based PVEH stack can operate reliably under harsh environmental conditions, since the compressive strength of the PZT stack is much higher than its tensile strength.

#### 4 Comparative Study 2: DACM-Based PVEH Stack and Conventional PZT Stack

This section is devoted to the comparison between the DACM-based PVEH and conventional PZT stacks. The DACM-based PVEH stack utilizes two-way compressive loadings, while conventional PZT stacks employ one-way compressive loadings directly [20, 23].

For the comparative study two, the simulation cases are summarized in Table 6. The same volume of the piezoelectric layers is used for the cases IV, V, and VI. The frequency of the dynamic force is 2.75 Hz. Figure 10 shows the dynamic force for the cases IV, V, and VI. For the case IV, a two-way compressive loading can be achieved by the DACM, as explained in Sect. 3. For the conventional PZT stacks, a one-way compressive loading only with no tension is applied in the case V, while, a compressive loading in a pre-strained condition is applied in the case VI.

The simulation results are summarized in Table 7. The mean values of the output electric power for the cases IV, V, VI are 19.6  $\mu$ W, 16.6  $\mu$ W, and 12.3  $\mu$ W, respectively. For the cases IV, V, and VI, the optimal external electrical resistances to generate the maximum output electric power are found as 24.7 k $\Omega$ , 43.7 k $\Omega$  and 52.2 k $\Omega$ , respectively, as shown in Fig. 11. As shown in Fig. 11, compared to conventional PZT stacks (cases V and VI), the DACM-based PVEH stack (case IV) can generate the higher output electric power with the same volume of the piezoelectric layers, since two peak values of the dynamic force appear per one cycle by converting base excitation into an elevated two-way compressive loading. The superiority of the DACM-based PVEH stack can be also demonstrated by the frequency responses for the cases IV, V, and VI in Fig. 12. It should be noted that the values of the output electric power at each excitation frequency in Figs. 11 and 12 are calculated by taking a time average for one cycle.

Figure 13 shows the simulation results of the cases IV, V, and VI. For the case IV, the stress and voltage profiles are similar to the dynamic force profile. For the case V, however, the stress profile is different from the dynamic force profile due to the stress release for the duration of zero force (no tension). For this duration, the output voltage generated by the

**Table 6** Simulation cases: DACM-based PVEH stack versus conventional PZT stack

	Case IV	Case V	Case VI
Mechanism	DACM-based PVEH stack	Conventional PZT stack	
Geometric dimensions	The number of PZT layers: 110 Size of a PZT layer: 5(L)×5(W)×0.127(T) mm		
Frequency	2.75 Hz		
Force amplitude	Max. -50 N (two-way compressive load)	Max. -50 N (one-way compressive load with no tension)	-25±25 N (one-way compressive load with pre-strain)

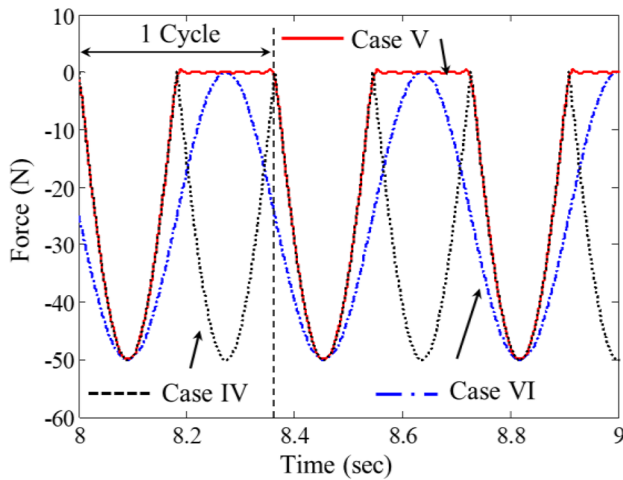


**Fig. 10** Dynamic forces applied to the DACM-based PVEH stack (case IV) and conventional PZT stacks (cases V and VI)

conventional PZT stack (case V) is affected by a time constant [2], which is the time required to charge the capacitor. The time constant leads to the electrical damping effect [30], thereby reducing the magnitude of the output voltage.

In addition, the output electric power generated by the DACM-based PVEH stack (case IV) is higher than that by the conventional PZT stack (case VI) using the one-way compressive load under a pre-strain condition, as shown in Fig. 13. Even though the range of the output voltage for the cases IV and VI is comparable to each other, the output electric power generated by the DACM-based PVEH stack (case IV) is larger than that by the conventional PZT stack (case VI) because the optimal external electrical resistances are different. It is thus confirmed that without any amplification mechanism, the

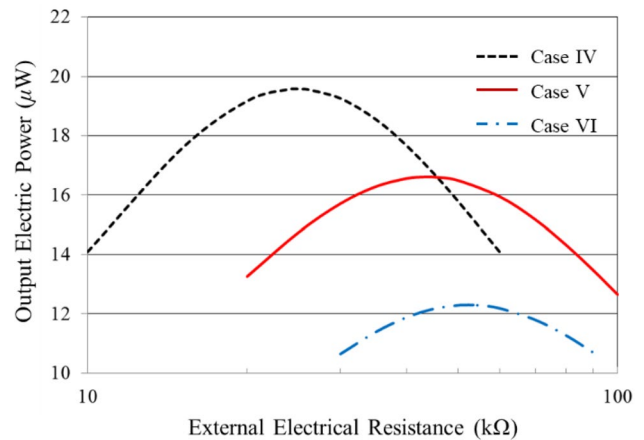


**Fig. 11** Output electric power with respect to external electrical resistances: Cases IV, V, and VI

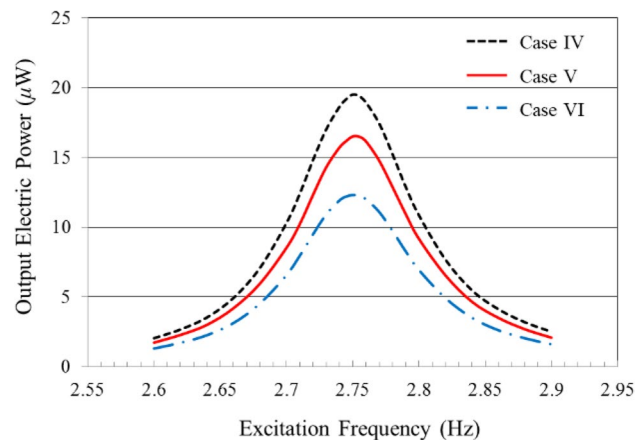
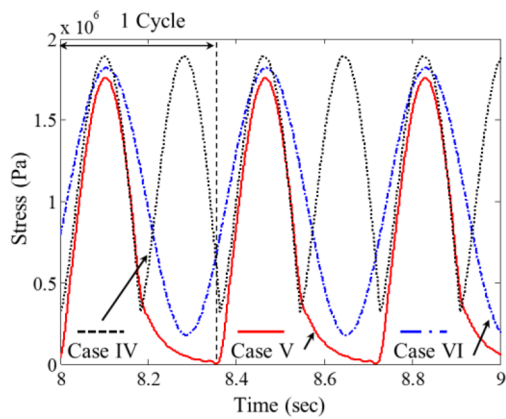


**Fig. 12** Frequency response for the output electric power: Cases IV, V, and VI

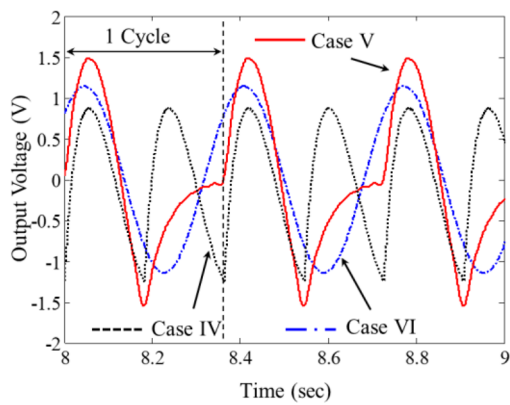
**Table 7** Simulation results of the comparison between the DACM-based PVEH and conventional PZT stacks

Performance	Case IV	Case V	Case VI
Optimal external electrical resistance	24.7 kΩ	43.7 kΩ	52.2 kΩ
Maximum stress	1.89 MPa	1.77 MPa	2.10 MPa
Output voltage range	-1.25 V ~ -0.87 V	-1.55 V ~ -1.48 V	-1.14 V ~ -1.14 V
Output electric power (time average)	19.6 µW	16.6 µW	12.3 µW

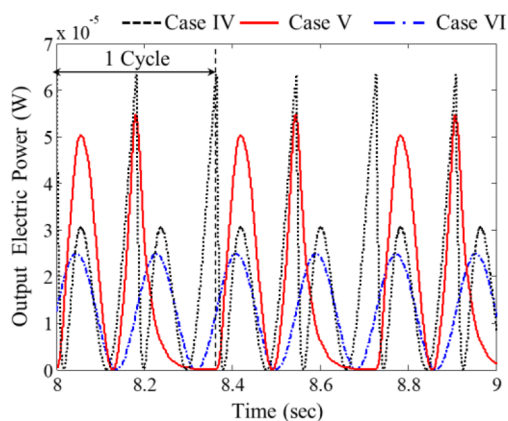




(a) Magnitude of compressive stress



(b) Output voltage



(c) Output electric power

**Fig. 13** Simulation results: Cases IV, V, and VI

DACM-based PVEH stack using two-way compressive loadings can generate more the output electric power in a time average sense than the conventional PZT stacks.

## 5 Conclusion

This study newly proposes an innovative piezoelectric vibration energy harvesting (PVEH) mechanism for 33-mode operation, namely a double acting compression mechanism (DACM)-based PVEH stack. The DACM converts base excitation into an elevated two-way compressive loading, thereby exploiting effectively the large magnitude of forces under the stress constraint on the compressive strength of the PZT stack. The electroelastically-coupled analytical model was used to predict the output performances of the DACM-based PVEH stack under the assumption of the damped SDOF system.

The comparative study is performed to verify the effectiveness of the DACM-based PVEH stack over other mechanisms. It can be concluded from the results that compared to conventional PZT stacks, the DACM-based PVEH stack can generate the higher output electric power with the same volume of the piezoelectric layers, since two peak values of the dynamic force appear per one cycle by converting base excitation into an elevated two-way compressive loading. In addition, since the compressive strength of the PZT stack is much higher than its tensile strength, the DACM-based PVEH stack can operate reliably under harsh environmental conditions. This implies that the large magnitude of dynamic forces can be applied to generate more the output electric power.

**Acknowledgements** This research was partially supported by the Main Project of Korea Institute of Machinery and Materials (Project Code: NK213E). This research was also supported by the National Research Council of Science & Technology (NST) grant by the Korea Government (MSIT) (No. CAP-17-04-KRISS).

## References

- Kim, J. E., Kim, H., Yoon, H., Kim, Y. Y., & Youn, B. D. (2015). An energy conversion model for cantilevered piezoelectric vibration energy harvesters using only measurable parameters. *International Journal of Precision Engineering and Manufacturing-Green Technology*, 2(1), 51–57.
- Cui, J., Yoon, H., & Youn, B. D. (2018). An omnidirectional biomechanical energy harvesting (OBEH) sidewalk block for a self-generative power grid in a smart city. *International Journal of Precision Engineering and Manufacturing-Green Technology*, 5(4), 507–517.
- Erturk, A., & Inman, D. J. (2008). On mechanical modeling of cantilevered piezoelectric vibration energy harvesters. *Journal of Intelligent Material Systems and Structures*, 19(11), 1311–1325.
- Yoon, H., Youn, B. D., & Kim, H. S. (2016). Kirchhoff plate theory-based electromechanically-coupled analytical model considering inertia and stiffness effects of a surface-bonded piezoelectric patch. *Smart Materials and Structures*, 25(2), 025017.

5. Kim, H. S., Kim, J.-H., & Kim, J. (2011). A review of piezoelectric energy harvesting based on vibration. *International Journal of Precision Engineering and Manufacturing*, 12(6), 1129–1141.
6. Usharani, R., Uma, G., & Umopathy, M. (2016). Design of high output broadband piezoelectric energy harvester with double tapered cavity beam. *International Journal of Precision Engineering and Manufacturing-Green Technology*, 3(4), 343–351.
7. Sodano, H. A., Inman, D. J., & Park, G. (2005). Comparison of piezoelectric energy harvesting devices for recharging batteries. *Journal of Intelligent Material Systems and Structures*, 16(10), 799.
8. Yoon, H., & Youn, B. D. (2014). Stochastic quantification of the electric power generated by a piezoelectric energy harvester using a time-frequency analysis under non-stationary random vibrations. *Smart Materials and Structures*, 23(4), 045035.
9. Roundy, S., Leland, E. S., Baker, J., Carleton, E., Reilly, E., Lai, E., et al. (2005). Improving power output for vibration-based energy scavengers. *Pervasive Computing*, 4(1), 28–36.
10. Anton, S. R., & Sodano, H. A. (2007). A review of power harvesting using piezoelectric materials (2003–2006). *Smart Materials and Structures*, 16(3), 1.
11. Yoon, H., Kim, M., Park, C.-S., & Youn, B. D. (2018). Time-varying output performances of piezoelectric vibration energy harvesting under nonstationary random vibrations. *Smart Materials and Structures*, 27(1), 015004.
12. Goldschmidtboeing, F., & Woias, P. (2008). Characterization of different beam shapes for piezoelectric energy harvesting. *Journal of Micromechanics and Microengineering*, 18(10), 104013.
13. Lee, S., Youn, B. D., & Jung, B. C. (2009). Robust segment-type energy harvester and its application to a wireless sensor. *Smart Materials and Structures*, 18(9), 095021.
14. Jung, B. C., Yoon, H., Oh, H., Lee, G., Yoo, M., et al. (2016). Hierarchical model calibration for designing piezoelectric energy harvester in the presence of variability in material properties and geometry. *Structural and Multidisciplinary Optimization*, 53(1), 161–173.
15. Roundy, S., Wright, P. K., & Rabaey, J. (2003). A study of low level vibrations as a power source for wireless sensor nodes. *Computer Communications*, 26(11), 1131–1144.
16. Sodano, H. A., Park, G., & Inman, D. J. (2004). Estimation of electric charge output for piezoelectric energy harvesting. *Strain*, 40(2), 49–58.
17. Chen, S. N., Wang, G. J., & Chien, M. C. (2006). Analytical modeling of piezoelectric vibration-induced micro power generator. *Mechatronics*, 16(7), 379–387.
18. Xu, T., Siochi, E. J., Kang, J. H., Zuo, Lei, Zhou, W., Tang, X., & Jiang, X. (2011). A Piezoelectric PZT ceramic Multilayer Stack for Energy Harvesting under Dynamic Forces. In: *Proceedings of the ASME 2011 International Design Engineering Technical Conference and Computers and Information in Engineering Conference*.
19. Xu, T., Siochi, E. J., Kang, J. H., Zuo, L., Zhou, W., Tang, X., et al. (2013). Energy harvesting using a pzt ceramic multilayer stack. *Smart Materials and Structures*, 22(6), 065015.
20. Feenstra, J., Granstrom, J., & Sodano, H. (2008). Energy harvesting through a backpack employing a mechanically amplified piezoelectric stack. *Mechanical Systems and Signal Processing*, 22(3), 721–734.
21. Song, H., Kim, H., Kang, C., Kim, H., Yoon, S., & Jeong, D. (2009). Multilayer piezoelectric energy scavenger for large current generation. *Journal of Electroceramics*, 23(2), 301–304.
22. Yuan, J., Shan, X., Xie, T., & Chen, W. (2010). Modeling and improvement of a cymbal transducer in energy harvesting. *Journal of Intelligent Material Systems and Structures*, 21(8), 765–771.
23. Lee, A., Wang, Y., & Inman, D. J. (2014). Energy harvesting of piezoelectric stack actuator from a shock event. *Journal of Vibration and Acoustics*, 136(1), 011016.
24. Zhao, S. (2013). Energy harvesting from random vibrations of piezoelectric cantilevers and stacks. PhD thesis, *Georgia Institute of Technology*.
25. Morgan Advanced Materials website. <http://www.morgantechnicalceramics.com>. Accessed 1 Feb 2019.
26. PIECO.COM website. <https://piezo.com>. Accessed 1 Feb 2019.
27. Flynn, A. M., & Sanders, S. R. (2002). Fundamental limits on energy transfer and circuit considerations for piezoelectric transformers. *IEEE Transactions on Power Electronics*, 17(1), 8–14.
28. Inman, D. J. (2013). *Engineering vibration* (4th ed.). Pearson Education, Inc., Upper Saddle River, NJ.
29. Lee, S., & Youn, B. D. (2011). A design and experimental verification methodology for an energy harvester skin structure. *Smart Materials and Structures*, 20(5), 057001.
30. Keawboonchuay, C., & Engel, T. G. (2003). Electrical power generation characteristics of piezoelectric generator under quasi-static and dynamic stress conditions. *IEEE Transactions on Ultrasonics, Ferroelectrics, and Frequency Control*, 50(10), 1377–1382.

**Publisher's Note** Springer Nature remains neutral with regard to jurisdictional claims in published maps and institutional affiliations.



**Byung C. Jung** is a Senior Researcher at Korea Institute of Machinery and Materials. He received his B.S. degree in mechanical engineering from Hanyang University, Korea, his M.S. degree in mechanical engineering from KAIST, Korea, and his Ph.D. in reliability engineering from the University of Maryland-College Park, USA, in 2011. His research interests are seismic qualification, design of energy harvesting device and reliability-based optimization.



**Heonjun Yoon** is a Postdoctoral Research Associate in the Department of Mechanical and Aerospace Engineering, Seoul National University, Seoul, Republic of Korea. Dr. Yoon received a Ph.D. degree from Seoul National University in 2018. Dr. Yoon was the recipient of two Best Thesis Awards from the KSME (2013 and 2018); several Best Paper Awards from the BAMN (2013), the KSNVE (2014), the ENGE (2016), and the KSME (2018); Featured Article from *Smart Materials*

and *Structures* (2014); the 1st Place Winner in the Student Paper Competition of the KSME (2016); Bronze Prize from KSME-SEMES Open Innovation Challenge (2016); Outstanding Doctoral Dissertation Award from the Department of Mechanical and Aerospace Engineering at Seoul National University (2018); and Young Scientist Award from the ASSMO (2018).